STRUCTURAL SCIENCE
CRYSTAL ENGINEERING
MATERIALS

ISSN: 2052-5206
journals.iucr.org/b

Structural, energetic and spectroscopic studies of new luminescent complexes based on 2-(2′-hydroxyphenyl)imidazo[1,2-*a*]pyridines and 1,2-phenylenediboronic acid

Sylwia E. Kutniewska, Katarzyna N. Jarzembska, Radosław Kamiński, Anton J. Stasyuk, Daniel T. Gryko and Michał K. Cyrański

Acta Cryst. (2018). B**74**, 725–737

Acta Cryst B
STRUCTURAL SCIENCE
CRYSTAL ENGINEERING
MATERIALS
ISSN 2052-5206

Structural, energetic and spectroscopic studies of new luminescent complexes based on 2-(2′-hydroxyphenyl)imidazo[1,2-*a*]pyridines and 1,2-phenylenediboronic acid

Sylwia E. Kutniewska,[a] Katarzyna N. Jarzembska,[a]* Radosław Kamiński,[a] Anton J. Stasyuk,[b] Daniel T. Gryko[c] and Michał K. Cyrański[a]

[a]Department of Chemistry, University of Warsaw, Żwirki i Wigury 101, Warsaw 02-089, Poland, [b]Institute of Computational Chemistry and Catalysis, Department of Chemistry, University of Girona, C/M. Aurèlia Capmany 69, Girona 17003, Spain, and [c]Institute of Organic Chemistry, Polish Academy of Sciences, Kasprzaka 44/52, Warsaw 01-224, Poland. *Correspondence e-mail: katarzyna.jarzembska@gmail.com

Received 28 August 2018
Accepted 1 November 2018

Edited by M. Dusek, Academy of Sciences of the Czech Republic, Czech Republic

Keywords: luminescent boron complexes; X-ray diffraction; periodic calculations; time-dependent density functional theory; TDDFT; UV–Vis spectroscopy; transferred aspherical atom model (TAAM) refinement; spectroscopic properties.

CCDC references: 1846570; 1846571; 1846572; 1846573; 1846574

Supporting information: this article has supporting information at journals.iucr.org/b

Three new blue-luminescent complexes of selected imidazo[1,2-*a*]pyridine derivatives and 1,2-phenylenediboronic acid have been synthesized and structurally characterized using single-crystal X-ray diffraction. Additionally, the crystal structures of two of the (*N*,*O*)-donor compounds have been evaluated for the first time. The crystal packing and molecular motifs observed in the studied crystals have been thoroughly analysed, including computational studies, and are also discussed within the context of analogous systems reported in the literature. It appears that the new compounds form different crystal networks with regard to the asymmetric unit content and packing, although some similarities can be found. In all cases a typical centrosymmetric dimer bound via boronic acid groups is formed, characterized by an interaction energy of about −80 kJ mol^{-1}, while the 2-(2′-hydroxyphenyl)imidazo[1,2-*a*]pyridine complex and its methoxy derivative form solvate structures, somewhat resembling the previously studied 8-oxyquinolinate analogues. As far as the spectroscopic properties are concerned, the lowest energy excitation observed in the studied complexes is based on the highest occupied molecular orbital–lowest unoccupied molecular orbital transition, and both these molecular orbitals are centred predominantly on the (*N*,*O*)-donor species according to the results of time-dependent density functional theory. Thus, the charge transfer observed for the 8-oxyquinolinate equivalents does not occur in these cases. Consequently, the spectroscopic behaviour of the series is very much comparable with that of the parent imidazo[1,2-*a*]pyridine derivatives, if the excited-state intramolecular proton-transfer process does not take place, as shown by the absorption and emission spectra collected in toluene and acetone solutions. Complexation causes a reduction in the Stokes shift compared with the respective (*N*,*O*)-donor molecules.

1. Introduction

New inexpensive functional materials with desired properties, such as photoactive substances applicable as sensors, biomarkers, optoelectronic devices *etc.* (Grätzel, 2009; Alibabaei *et al.*, 2013; Kamtekar *et al.*, 2010), are nowadays of both top scientific and technological interest. Boron-containing species, *e.g.* low-cost luminescent borinic-type complexes (R_2BQ) (Wesela-Bauman *et al.*, 2013; Knox *et al.*, 2006; Anderson *et al.*, 2000; Wang & Weck, 2005; Lin *et al.*, 2014; Qin *et al.*, 2006; Nagata & Chujo, 2008; Cui & Wang, 2006; Li & Jäkle, 2009; Kappaun *et al.*, 2006), and the 9,10-dihydro-9,10-diboraanthracene-based systems (Jarzembska *et al.*, 2015; Durka *et al.*, 2014; Luliński *et al.*, 2013) fulfil these criteria.

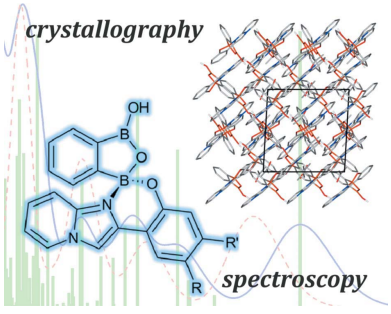

Quite recently, we have also introduced new easily synthesized luminescent complexes based on *ortho*-phenylenediboronic acid (**odba**) and 8-hydroxyquinoline (Jarzembska, Kamiński, Durka, Kubsik *et al.*, 2017).

As **odba**, in contrast with the isomeric *para*- and *meta*-phenylenediboronic acids, readily forms complexes with various (*N*,*O*)-donor species (Jarzembska, Kamiński, Durka, Kubsik *et al.*, 2017), we decided to verify whether such a reaction also proceeds smoothly with a series of recently synthesized fluorescent imidazo[1,2-*a*]pyridine derivatives, which are shown in Scheme 1 (Stasyuk *et al.*, 2012), and if so, how the complexation influences their spectroscopic properties. The choice of these systems is dictated primarily by their 'local' similarity to the previously successfully used 8-hydroxyquinoline and the described fluorescent behaviour (Mutai *et al.*, 2013, 2008; Stasyuk *et al.*, 2012). It is worth emphasizing, however, that on the top of their emissive properties imidazo[1,2-*a*]pyridines also exhibit a wide range of biological activities. Consequently, they have already found numerous applications in the pharmaceutical industry thanks to their antiviral (Gueiffier *et al.*, 1998), anti-inflammatory (Márquez-Flores *et al.*, 2012), analgesic (Ribeiro *et al.*, 1998), antipyretic (Abignente, 1991), anti-ulcer (Corona *et al.*, 1981) and antibacterial properties (Starr *et al.*, 2009). Furthermore, imidazo[1,2-*a*]pyridines with the 2-hydroxyphenyl substituent can be classified as excited-state intramolecular proton transfer (ESIPT) compounds. The proton transfer is responsible for their interesting luminescent properties, such as a large Stokes shift, and can be tuned via the character of the phenyl-ring substituent and the choice of solvent. In consequence, they can be used as laser dyes, fluorescence sensors, molecular switches *etc.*

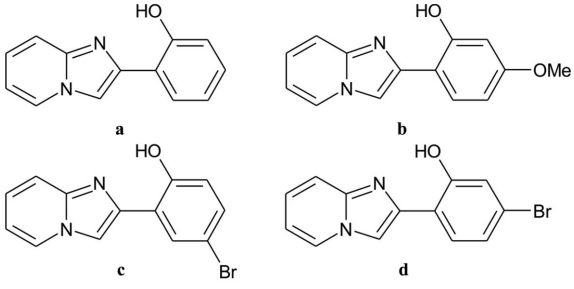

Scheme 1

Scheme 2 shows a schematic representation of the reaction of **odba** with the imidazo[1,2-*a*]pyridines **a**–**d** illustrated in Scheme 1, leading to the formation of the studied boron complexes labelled **odba-x**, where **x** = **a**–**d**.

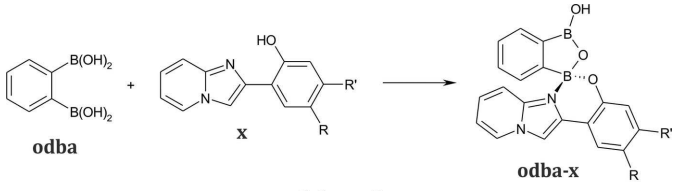

Scheme 2

In this contribution we present the crystal structures of three new *ortho*-phenylenediboronic acid complexes with fluorescent imidazo[1,2-*a*]pyridines, namely **odba-a**, **odba-b** and **odba-d** (Schemes 1 and 2), and also the crystal structures of the **b** and **c** substrates. The studied systems have been thoroughly analysed both structurally and energetically. Additionally, their spectroscopic properties in solution have been examined experimentally and modelled theoretically using time-dependent density functional theory (TDDFT) computations.

2. Experimental

2.1. Crystal synthesis

The **odba** compound and the 2-(2′-hydroxyphenyl)-imidazo[1,2-*a*]pyridines **a**–**d** were obtained according to the literature procedures (Durka *et al.*, 2013; Stasyuk *et al.*, 2012). The syntheses of complexes **odba-a**, **odba-b**, **odba-c** and **odba-d** were carried out as described in our recent paper (Jarzembska, Kamiński, Durka, Kubsik *et al.*, 2017). Single crystals of **odba-a** and **odba-b** were prepared by slow evaporation at room temperature from concentrated acetone solutions containing equimolar amounts of **odba** and the respective (*N*,*O*)-donor compound. The **odba-d** compound was crystallized via chloroform diffusion into a concentrated methanol solution of the complex. However, in spite of numerous trials, we have not succeeded in growing **odba-c** crystals suitable for further X-ray diffraction studies. Similar to **odba-d**, single crystals of the **b** and **c** substrates were obtained using the chloroform/methanol diffusion method.

2.2. X-ray crystallography

All single-crystal X-ray measurements were carried out on a Bruker AXS D8 VENTURE diffractometer equipped with a CMOS detector and a low-temperature open-flow device to keep the samples at 100 K. Data-collection strategies, structure determination and optimization, unit-cell determination, raw diffraction image integration and data scaling were all performed using the appropriate algorithms implemented in the *APEX3* diffractometer software (Bruker, 2015).

All structures were solved using a charge-flipping method (Oszlányi & Sütő, 2004, 2005; Palatinus, 2013) as implemented in the *SUPERFLIP* program (Palatinus & Chapuis, 2007), and initially refined with the *JANA* package (Petříček *et al.*, 2014) within the independent atom model (IAM) approximation. Subsequently, transferred aspherical atom model (TAAM) refinements were performed with *JANA* with the aid of a locally modified version of the University at Buffalo Data Bank (Jarzembska & Dominiak, 2012), based on the Hansen–Coppens multipole model (Hansen & Coppens, 1978). Such an approach gives excellent results in terms of geometry (Jarzembska *et al.*, 2012) and displacement parameters (Jarzembska *et al.*, 2014), and provides molecular geometries of sufficient quality to perform subsequent periodic computations (where needed, the disorder was removed). For more details regarding the refinement see the supporting information (additional references: Macchi & Coppens, 2001; Su & Coppens, 1998; Dominiak *et al.*, 2007; Volkov *et al.*, 2004; Allen *et al.*, 1987; Allen & Bruno, 2010). CIF files for each refine-

Table 1
Selected structural parameters for the newly determined crystal structures of imidazo[1,2-*a*]pyridines.

For more details, see the supporting information.

Structure	**b**	**c**
Formula	$C_{14}H_{12}N_2O_2$	$C_{13}H_9BrN_2O$
Crystal system	Orthorhombic	Monoclinic
Space group	*Pbca* (No. 61)	$P2_1/c$ (No. 14)
a (Å)	14.5448 (2)	12.8423 (7)
b (Å)	6.5214 (4)	7.0971 (4)
c (Å)	23.8246 (6)	12.6239 (7)
α (°)	90	90
β (°)	90	107.1883 (16)
γ (°)	90	90
V (Å^3)	2259.82 (15)	1099.19 (11)
Z	8	4
$R(F)$ [$I > 3\sigma(I)$]	0.0328	0.0251
$R(F)$ (all data)	0.0479	0.0457
$wR(F^2)$ (all data)	0.0751	0.0500
S (all data)	1.70	1.21
$\Delta\rho_{min}$, $\Delta\rho_{max}$ (e Å^{-3})	−0.32, +0.25	−0.45, +0.56
CSD refcode	1846570	1846571

ment are present in the supporting information, or can be retrieved from the Cambridge Structural Database (CSD; Groom *et al.*, 2016) (for deposition numbers, see Tables 1 and 3, and Table 1S in the supporting information). All raw data and associated refinement files are available under the DOI 10.18150/repod.5973048.

2.3. Theoretical computations

Periodic calculations yielding the crystal cohesive-energy values were conducted using the *CRYSTAL09* program package (Dovesi *et al.*, 2005, 2009) at the DFT(B3LYP) level of theory (Perdew, 1986; Becke, 1988; Lee *et al.*, 1988) applying the pobTZVP basis set (Peintinger *et al.*, 2013). The evaluation of Coulomb and exchange series was controlled by five thresholds, set arbitrarily to the values of 10^{-7}, 10^{-7}, 10^{-7}, 10^{-7} and 10^{-25}, respectively, and the shrinking factor was equal to 8. Both Grimme empirical dispersion correction (Grimme, 2006, 2004) and correction for basis-set superposition error (Boys & Bernardi, 1970; Simon *et al.*, 1996) (BSSE) were applied. The *CRYSTAL* input files were prepared with the *CLUSTERGEN* program (Kamiński *et al.*, 2013).

The intermolecular interaction energies were evaluated using the *GAUSSIAN09* package (Frisch *et al.*, 2009). The DFT(B3LYP)/6-311++G** (Becke, 1988; Perdew, 1986; Lee *et al.*, 1988; Krishnan *et al.*, 1980; Clark *et al.*, 1983; McLean & Chandler, 1980) method was employed with the Grimme empirical dispersion correction (Grimme, 2006, 2004), modified by the Becke–Johnson damping function (Grimme *et al.*, 2011, 2010) and correction for BSSE (Boys & Bernardi, 1970; Simon *et al.*, 1996). The automatic generation of molecular motifs was accomplished with the *CLUSTERGEN* program (Kamiński *et al.*, 2013).

Time-dependent density functional theory (TDDFT) computations were conducted using the *GAUSSIAN09* package at the DFT(PBE0)/6-31G** (Adamo & Barone, 1999; Perdew *et al.*, 1996; Dill & Pople, 1975; Hariharan & Pople, 1973; Hehre *et al.*, 1972) and DFT(B3LYP)/6-311++G** levels of theory. Optimizations of gas-phase molecular geometries were performed at the DFT(B3LYP)/6-311++G** level of theory. The *GAUSSSUM* program (O'Boyle *et al.*, 2008) was used to draw the UV–Vis spectra based on the TDDFT results.

2.4. Optical spectroscopy

Solution–sample absorbance measurements were performed using a Shimadzu UV-2401PC spectrometer with a spectral resolution of 1 nm. The spectra were measured in both toluene and acetone. Steady-state fluorescence measurements were conducted using a Perkin–Elmer spectrofluorometer (model LS55). All solution samples were excited using either 315 or 330 nm wavelengths, and their emission was measured in an interval ranging from 300 to 700 nm.

3. Results and discussion

3.1. New crystal structures of selected 2-(2′-hydroxyphenyl)imidazo[1,2-*a*]pyridines

Prior to the synthesis of the desired complexes, we focused our attention on the (*N*,*O*)-donor compounds. To date only a few crystal structures of analogous 2-(2′-hydroxyphenyl)-imidazo[1,2-*a*]pyridines can be found in the literature (Stasyuk, Bultinck *et al.*, 2016; Stasyuk, Cywiński & Gryko, 2016; Mutai *et al.*, 2008, 2016, 2014; An *et al.*, 2016; Salunke *et al.*, 2012; Balijapalli & Iyer, 2015; Wu *et al.*, 2017). Among them, two compounds crystallized by some of us (Stasyuk, Bultinck *et al.*, 2016; Stasyuk, Cywiński & Gryko, 2016) contained either a fluorine atom or a methyl group at the *R* substituent position shown in Scheme 2. Out of the four

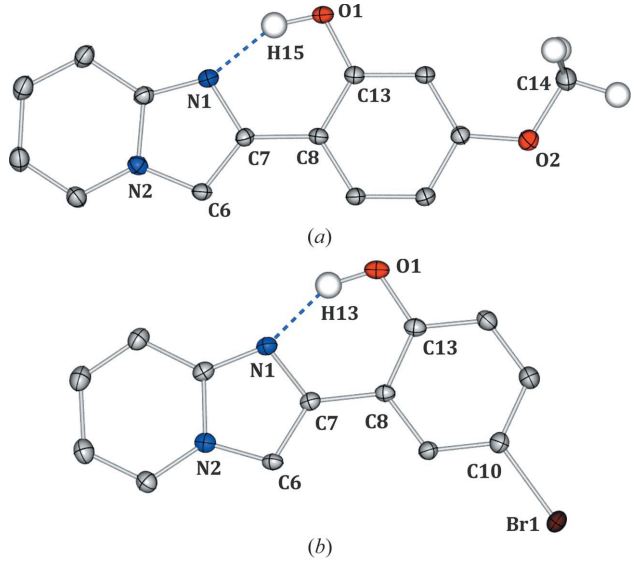

Figure 1
Labelling of atoms and representation of their displacement parameters as probability ellipsoids (50% probability level) after the final TAAM refinement for the molecules of (*a*) **b** and (*b*) **c**. Some H atoms have been omitted for clarity.

systems of this kind selected for the purpose of the current study, only in the case of **b** (R = H, R' = OMe) and **c** (R = Br, R' = H) were we able to obtain crystals suitable for further X-ray diffraction studies (Fig. 1). It appears that **c**, similar to the literature-reported fluorine and methyl derivatives (Stasyuk, Bultinck *et al.*, 2016), crystallizes in the monoclinic space group $P2_1/c$ (all three systems have the R substituent at the *para*-position with respect to the hydroxyl group). Furthermore, these compounds form comparable molecular networks in the solid state. In general, they create 'zigzag' molecular patterns visible when looking along the [100] direction (Fig. 2*a*), and also readily distinguishable molecular layers parallel to the (011) crystal plane. In the latter case, the R substituent points towards the space in between such layers (Fig. 2*b*).

Considering the size of the R substituent, a methyl group compares better to a bromine than to a fluorine atom regarding the corresponding volumes calculated based on the atomic van der Waals (vdW) radii (Zhao *et al.*, 2003) (fluorine volume 13.31 Å^3, chlorine 22.45 Å^3 and bromine 26.52 Å^3, whereas that of a methyl group is 21.56 Å^3, half of the vdW volume of an ethane molecule). These numbers also show that a methyl group is most comparable to a chlorine atom in this respect. This observation is well reflected in many crystal engineering papers dealing with the 'methyl-to-chlorine substitution' effect and its impact on the resulting crystal structures (Mondal *et al.*, 2012; Desiraju & Sarma, 1986; Edwards *et al.*, 2001). The size of a bromine atom, though, is also not much larger than that of a methyl group. Indeed, both the methyl and bromine 2-(2′-hydroxyphenyl)imidazo[1,2-*a*]pyridine derivatives form isostructural crystal structures (according to the IUCr definition; Authier, 2014). They all share the stronger intermolecular contact types, as indicated by Hirshfeld surface analysis (Spackman, 2013; Spackman & Jayatilaka, 2009) (supporting information). Nevertheless, in the case of the **c** compound additional short contacts are formed due to the slightly larger size of the bromine atom and its chemical character, namely weak interlayer C3—H3···Br1 contacts [H3···Br1 = 2.777 (10) Å, C3—H3···Br1 = 129.4 (9)°, interaction energy *ca* −5 kJ mol^{-1}], which are illustrated by fingerprint plots (Fig. 5S in the supporting information). In turn, although the fluorine-substituted analogue exhibits similar crystal packing (*i.e.* the spatial arrangement of molecules in its crystal structure is only seemingly the same), it is no longer isostructural with **c** and the methyl derivative. This is most probably due to the significantly smaller volume of the fluorine substituent, which imposes a somewhat different mutual orientation of the molecules, resulting in F···F interactions, as studied by some of us previously (Stasyuk, Bultinck *et al.*, 2016) (Fig. 3S). The volume of the molecular Hirshfeld surface calculated for the fluorine derivative is also the smallest among the analysed group (247.32 Å^3), while for **c** and the methyl derivative these values are very much alike (268.56 and 268.22 Å^3, respectively).

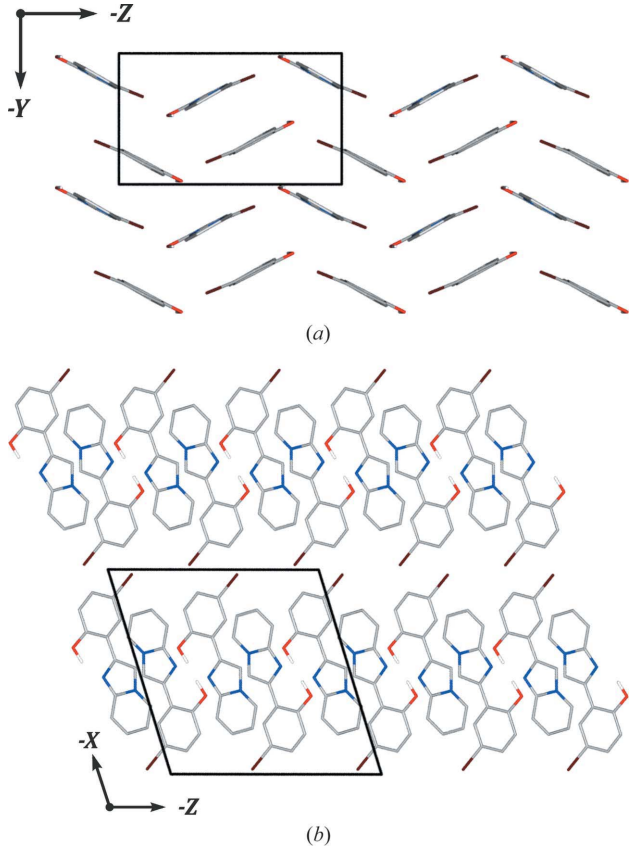

Figure 2
Crystal packing of the bromine derivative, **c**. (*a*) A view along the [100] direction and (*b*) a view along the [010] direction.

The methoxy derivative, **b**, thanks to the electronegative oxygen atom at the R' position, is more prone to forming hydrogen-bond-like intermolecular contacts, and thus some classical C3—H3···O2 and C12—H12···O2 interactions are present in its crystal structure (Fig. 4S). The *meta* methoxy substituent position with respect to the hydroxyl group and the more complex molecular network result in a significantly different crystal packing from that of the previously described systems, and also in higher symmetry (space group *Pbca*). The $d_{\rm norm}$ property mapped on the molecular Hirshfeld surface derived for **b** and the respective fingerprint plot (supporting information) show that the close intermolecular contacts are no shorter here than in the case of the remaining crystal structures, but they are more numerous, and the Hirshfeld surface volume is significantly smaller than that of the bromine and methyl derivatives, despite the bulkier methoxy substituent, which suggests a denser crystal packing (Fig. 3).

As far as the crystal-packing features are concerned, molecules of **b** form undulating layers parallel to the (101) crystal plane. Such layers consist of molecular chains formed via O2···H3 interactions and interconnected to one another by O1···C6 and other weak contacts (*e.g.* H···H and H···C). Adjacent layer motifs are stabilized mainly by H3···O1 interactions, and by contacts between methyl groups and five-membered aromatic ring fragments.

The most advantageous intermolecular interaction in the crystal structure of **c** (*ca* −73 kJ mol^{-1}) is found for the $\pi\cdots\pi$ interacting centrosymmetric molecular dimer. The distance

between the least-squares-derived planes of the two molecules is about 3.3 Å, whereas the centroid offset parameter is ∼2.1 Å. The interplanar distance is shorter here than for the fluorine equivalent (3.4 Å) and very much comparable with that found in the methyl derivative's crystal structure (3.3 Å). In turn, the centroid offset is least significant in the case of the fluorine analogue (1.7 Å) and largest for the methyl derivative (2.4 Å). Other more notably interacting molecular motifs include a second π-stacking-like motif in which the molecules are further apart, an edge-to-face type motif and a dimer linked via O1···H6 interactions. In the case of **b**, $\pi\cdots\pi$ stacking also plays a significant role in crystal stabilization, together with interactions engaging the two oxygen atoms (from the hydroxy and methoxy groups). The strongest interacting molecular dimer is characterized here by an energy of about −43 kJ mol^{-1} but a number of other motifs interact more strongly than −20 kJ mol^{-1}. Nevertheless, regarding the cohesive energy values (Table 2), there is almost no difference between the **b** and **c** crystal structures. This suggests that any deviation in the crystallization of the two systems results from either entropic or kinetic factors.

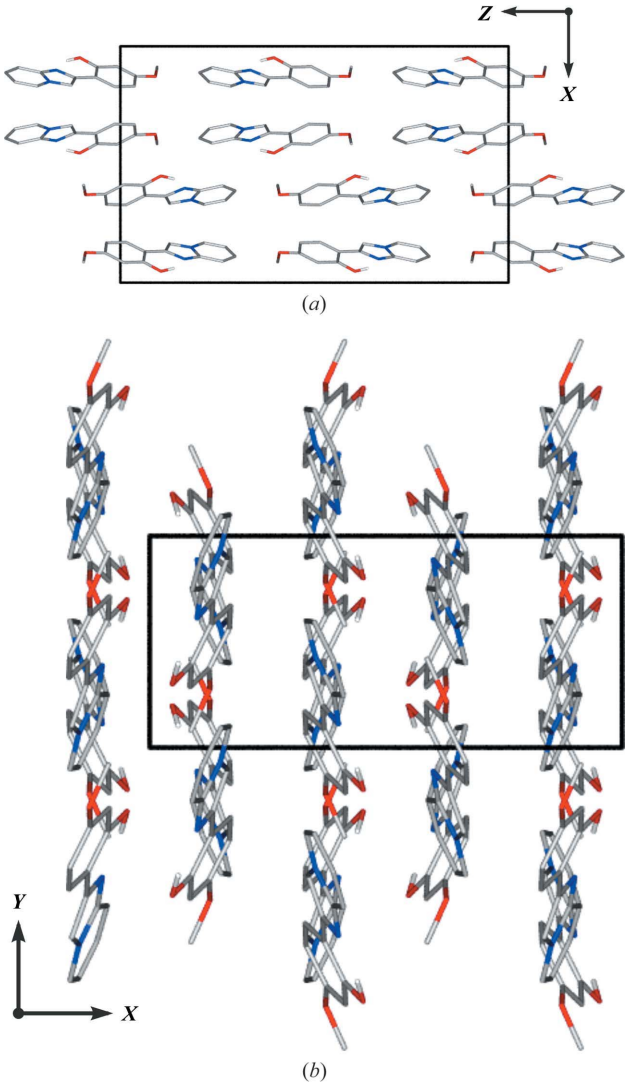

Figure 3
Crystal packing of the methoxy derivative, **b**. (*a*) A view along the [010] direction and (*b*) a view along the [001] direction.

Table 2
Cohesive energy values (E_{coh}) evaluated for the studied crystal structures (with the disorder removed if necessary) and for their 'no-solvent' equivalents (E_{coh}^{nosv}) [all at the DFT(B3LYP)/pobTZVP level and computed with the *CRYSTAL09* program].

Values are given for a single molecule or for one molecule with the corresponding number of solvent species.

Structure	E_{coh} (kJ mol^{-1})	E_{coh}^{nosv} (kJ mol^{-1})
b	−129.9	
c	−128.8	
odba-a	−242.6	−167.5
odba-b	−233.5	−194.5
odba-d	−208.6	

Theoretically calculated atomic electrostatic potential fitted charges (Table 2S) also do not show any significant differences influenced by the *R* or *R*′ substituents. It appears that the *R* substituent, whether CH_3, F, Cl, Br or OCH_3, does not affect the charge of atom O1 much with respect to the unsubstituted (*R* = H) case, whereas the *R*′ substituent from the analysed group always reduces the negative charge at O1, although the differences are still rather small. A similar observation can be made for atom N1. Therefore, it seems that the character of a given substituent and its location (*R* versus *R*′ position) matter more with respect to interactions with the solvent and the molecular arrangement in the solid-state form. These findings agree with the spectroscopic results obtained previously (Stasyuk *et al.*, 2012).

Finally, it should also be noted that, in agreement with Etter's rules (Etter, 1990), an intramolecular hydrogen bond between the hydroxyl group and atom N1 is formed in all the analysed 2-(2′-hydroxyphenyl)imidazo[1,2-*a*]pyridine crystal structures. This feature has consequences for the luminescence properties of the series in the solid state, facilitating ESIPT upon irradiation with UV light, which results in significantly red-shifted emission (see following sections).

3.2. Crystal structures of the studied complexes: general remarks

As far as the *ortho*-phenylenediboronic acid complexes with 2-(2′-hydroxyphenyl)imidazo[1,2-*a*]pyridines are concerned, three of them were crystallized successfully, *i.e.* **odba-a**, **odba-b** and **odba-d** (Fig. 4, Table 3). Each of these compounds forms a different crystal structure, unlike the previously investigated 8-oxyquinolinate complexes (Jarzembska, Kamiński, Durka, Kubsik *et al.*, 2017; Jarzembska, Kamiński, Durka & Kubsik, 2017). They vary regarding the space-group symmetry, packing and content of the asymmetric unit (ASU). The respective packing diagrams are shown in Fig. 5.

The **odba-a** compound crystallizes in the $P2_1$ space group with four complex molecules in the ASU and four acetone species. **Odba-b** also forms a monoclinic solvate structure, but here the ASU contains one complex molecule and half of a disordered acetone molecule, leading to the *C*2/*c* space group.

Table 3
Selected structural parameters for the studied **odba** complexes.

For more details, see the supporting information.

Structure	**odba-a**	**odba-b**	**odba-d**
Formula	$C_{19}H_{14}B_2N_2O_3\cdot C_3H_6O$	$2(C_{20}H_{16}B_2N_2O_4)\cdot C_3H_6O$	$C_{19}H_{13}B_2BrN_2O_3$
Crystal system	Monoclinic	Monoclinic	Triclinic
Space group	$P2_1$ (No. 4)	$C2/c$ (No. 15)	$P\overline{1}$ (No. 2)
a (Å)	10.7147 (11)	21.8035 (16)	8.9492 (7)
b (Å)	34.282 (3)	10.4647 (8)	14.5926 (12)
c (Å)	10.9168 (11)	19.3032 (14)	15.0762 (12)
α (°)	90	90	66.778 (3)
β (°)	93.176 (2)	111.794 (3)	82.477 (3)
γ (°)	90	90	86.204 (3)
V (Å^3)	4003.8 (7)	4089.6 (5)	1793.5 (3)
Z	8	4	2
$R(F)$ $[I > 3\sigma(I)]$	0.0548	0.0600	0.0480
$R(F)$ (all data)	0.1796	0.0732	0.1069
$wR(F^2)$ (all data)	0.1016	0.1541	0.1019
S (all data)	1.19	2.59	1.97
$\Delta\rho_{min}$, $\Delta\rho_{max}$ (e Å^{-3})	−0.71, +0.76	−0.43, +0.33	−0.79, +3.73
CSD refcode	1846572	1846573	1846574

Finally, the **odba-d** complex forms the crystal structure with the lowest space-group symmetry, $P\overline{1}$, where the ASU contains two complex molecules and no solvent species. Nevertheless, all three crystal structures under consideration share the main and usually best stabilized molecular motif, **D1**, which is a hydrogen-bonded dimer interacting via the boronic groups (Fig. 6 and Table 4). Such behaviour is analogous to that observed for the other reported structures of the **odba** luminescent complexes (Jarzembska, Kamiński, Durka, Kubsik *et al.*, 2017; Jarzembska, Kamiński, Durka & Kubsik, 2017). It is also worth noting here that the structures of **odba-a** and **odba-b** also resemble to some extent the previously published 8-hydroxyquinoline complexes in terms of packing (Jarzembska, Kamiński, Durka, Kubsik *et al.*, 2017; Jarzembska, Kamiński, Durka & Kubsik, 2017). Indeed, the planes defined by the **D1** motif, *i.e.* by B(O)OH···O(HO)B, share the same orientation in the whole crystal structure, which is roughly along the $(\overline{1}01)$ crystal planes. Consequently, the flat aromatic ring (*N*,*O*)-donor fragments are arranged parallel to the (101) crystal planes, forming a characteristic weave-like motif, clearly visible in the case of the **odba-b** structure (for the **odba-a** crystal structure this view is not that clear due to the multiple molecules in the ASU).

3.3. Structural motifs in the studied complexes

The main types of molecular dimer formed in the studied complexes are presented in Fig. 6 and the respective interaction energies are provided in Table 4.

In the case of the **odba-a** crystal structure, the large number of molecules present in the ASU hampers the analysis of molecular motifs. However, a number of dimers formed by the four distinguishable complex species are very alike and characterized by very similar energy values. Consequently, only representative motifs will be discussed. Except for the already mentioned classical synthon **D1** (average interaction energy −76.5 kJ mol^{-1}), **odba-a** also exhibits some other less well stabilized molecular arrangements. For instance, **D2** and **D4** are held by weak C—H···O and supplementary edge-to-face C—H··· π interactions between acid and ligand fragments, whereas the **D3** motif is mostly $\pi\cdots\pi$ interacting via the phenyl groups. Of these three, the **D4** dimer is the most energetically stabilized and **D2** the least. In addition, there are multiple dimeric motifs, the energies of which range from roughly −10 to −20 kJ mol^{-1} (in all cases C—H···O interactions play a dominant role).

Similar to **odba-a**, **odba-b** forms a **D1** motif of a comparable energy (−79 kJ mol^{-1}), and also **D2**-type and **D3′** dimers in its crystal structure. However, despite the structural resemblance, their overall energy is quite different from that calculated for the analogues present in the **odba-a** case. The less favourable energy value derived for the **D2** motif results from the lack of a C—H···π interaction. In addition, the much more advantageous interaction energy of **D3′** compared with the **D3** motif originates from a better coverage of the interacting (*N*,*O*)-

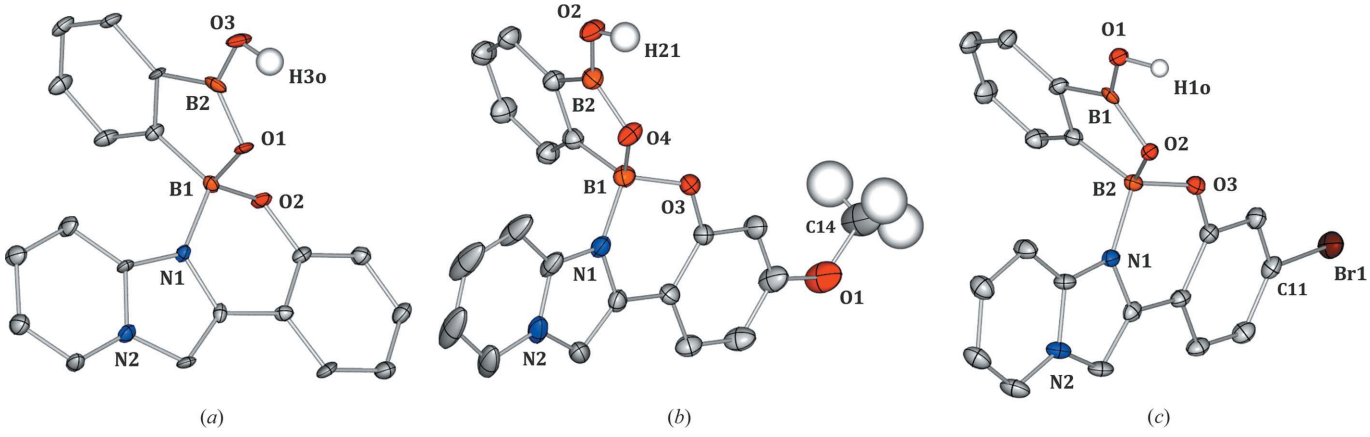

(*a*) (*b*) (*c*)

Figure 4
Labelling of atoms and representation of their displacement parameters as probability ellipsoids (50% probability level) after the final TAAM refinement for the molecules of (*a*) **odba-a**, (*b*) **odba-b** and (*c*) **odba-d**. In panels (*a*) and (*c*) only one representative molecule from the ASU is shown. Some H atoms and solvent molecules have been omitted for clarity.

donor ring fragments (all aromatic rings are involved in the interaction, Fig. 6) and a more preferential $\pi\cdots\pi$ interaction distance. The latter parameter amounts to about 3.4 Å for **D3′** (with a respective centroid offset of 1.0 Å), whereas a value of ~3.6 Å was encountered for **D3** (centroid offset 0.7 Å) in the **odba-a** crystal structure. As a result, **D3′** constitutes the most energetically stabilized dimer found in the studied crystal systems (*ca* −93 kJ mol^{-1}).

Apart from the described **D**-type motifs, there are two others worth mentioning that are present exclusively in this particular crystal structure, namely **X1** and **X2**. The **X1** dimer is formed by C—H$\cdots\pi$ interactions between the imidazo[1,2-

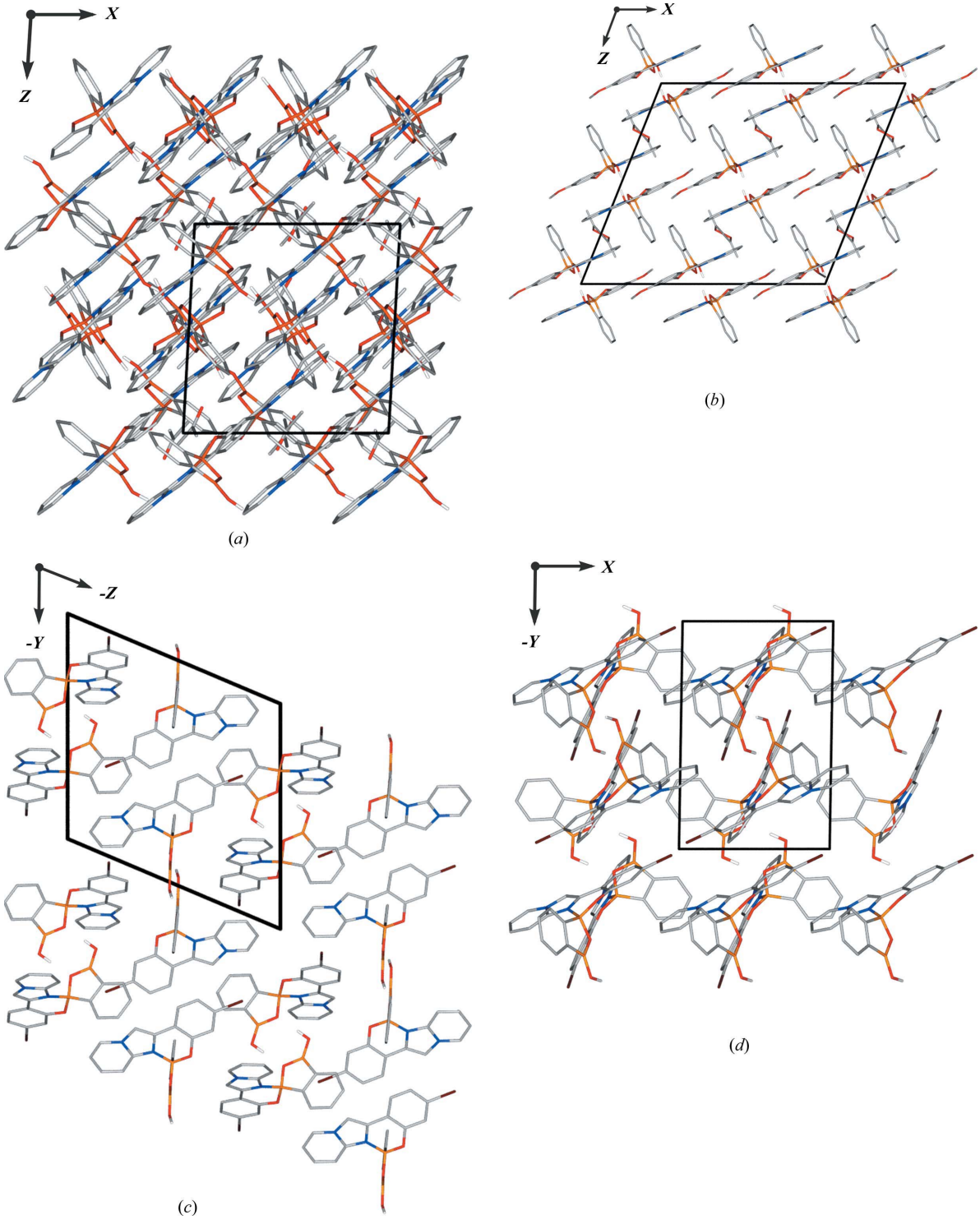

Figure 5
Crystal packing of the **odba** complexes. (*a*) **odba-a**, viewed along the [010] direction; (*b*) **odba-b**, viewed along the [010] direction; (*c*) **odba-d**, viewed along the [100] direction; (*d*) **odba-d**, viewed along the [001] direction.

Table 4
Interaction energy values E_{int} [computed at the DFT(B3LYP)/6-311++G** level of theory] and geometric parameters for selected weak interactions present in the studied crystal structures.

D and *A* denote interaction donor and acceptor, respectively. $X(\pi)$ stands for the closest atom involved in either D—H$\cdots\pi$ or $\pi\cdots\pi$ interactions. Dimers are labelled **D** or **X**, where **D** means that similar dimers are encountered in more than one studied crystal structure, and **X** the opposite.

Structure	Motif	E_{int} (kJ mol^{-1})	Selected interactions	D—H (Å)	H$\cdots A$ (Å)	$D\cdots A$ (Å)	D—H$\cdots A$ (°)
odba-a	**D1**	−76.86	O3—H3O$\cdots$O6	0.98 (3)	1.71 (3)	2.685 (3)	174 (3)
			O4—H4O$\cdots$O1	0.98 (3)	1.72 (3)	2.701 (3)	175 (3)
	D2	−32.76	C25—H25$\cdots$O11^{i}	1.08	2.38	3.207 (4)	132.22
			C24—H24$\cdots$O11^{i}	1.08	2.44	3.310 (4)	136.15
			C76—H76$\cdots$C24(π)^{ii}	1.08	2.84	3.845 (4)	154.95
	D3	−37.32	C11(π)$\cdots$C65(π)^{iii}			3.587 (5)	
			C12(π)$\cdots$C66(π)^{iii}			3.541 (5)	
			C13(π)$\cdots$C67(π)^{iii}			3.567 (5)	
	D4	−47.03	C4—H4$\cdots$C38(π)^{iv}	1.08	2.87	3.895 (5)	157.73
			C3—H3$\cdots$O5^{iv}	1.08	2.28	3.353 (4)	170.17
odba-b	**D1**	−79.12	O2—H21$\cdots$O4^{v}	0.980 (1)	1.73 (1)	2.703 (2)	174 (2)
	D2	−18.70	C9—H9$\cdots$O2^{vi}	1.08 (2)	2.50 (2)	3.556 (3)	165 (1)
			C6—H6$\cdots$O2^{vi}	1.081 (5)	2.747 (9)	3.748 (2)	154 (2)
	D3′†	−92.68	C11(π)$\cdots$C5(π)^{vii}			3.392 (2)	
			C12(π)$\cdots$C5(π)^{vii}			3.378 (2)	
	X1	−70.08	C4—H4$\cdots$C17(π)^{viii}	0.97 (5)	2.84 (4)	3.552 (5)	131 (2)
			C3—H3$\cdots$C18(π)^{viii}	1.07 (4)	2.84 (5)	3.696 (4)	137 (3)
			C3—H3$\cdots$C19(π)^{viii}	1.07 (4)	2.89 (4)	3.925 (4)	165 (3)
			C5(π)$\cdots$C5(π)^{viii}			3.359 (2)	
	X2	−44.06	C14—H14*C*$\cdots$C15(π)^{ix}	1.08 (3)	2.62 (4)	3.510 (6)	139 (2)
odba-d	**D1**	−79.96	O1—H1O$\cdots$O2^{x}	0.99 (2)	1.69 (2)	2.672 (2)	172 (2)
	D3	−71.50	C9(π)$\cdots$C9(π)^{xi}			3.140 (4)	
			C8(π)$\cdots$C9(π)^{xi}			3.389 (4)	
	X3	−53.39	C23—H23$\cdots$O5^{xii}	1.08 (3)	2.39 (2)	3.212 (3)	132 (2)
	X4	−54.73	C5—H5$\cdots$O6	1.08 (4)	2.20 (3)	3.163 (4)	147 (2)
			C5—H5$\cdots$C33(π)	1.08 (4)	2.87 (3)	3.865 (5)	154 (2)
			C6—H6$\cdots$C35(π)	1.09 (3)	2.76 (3)	3.842 (5)	171 (2)
			C6—H6$\cdots$C36(π)	1.09 (3)	2.66 (2)	3.612 (4)	146 (2)
			C6—H6$\cdots$C37(π)	1.09 (3)	2.79 (2)	3.585 (4)	130 (2)
	X5	−54.35	C25—H5O$\cdots$O1^{xiii}	1.082 (6)	2.37 (2)	3.343 (3)	149 (2)
			C3(π)$\cdots$C27(π)^{xiii}			3.350 (4)	
			C3(π)$\cdots$C32(π)^{xiii}			3.398 (4)	

Symmetry operations: (i) $x+1, y, z$; (ii) $x-1, y, z$; (iii) $-x, y+\frac{1}{2}, -z+1$; (iv) $x, y, z-1$; (v) $-x+1, -y+1, -z$; (vi) $x, y-1, z$; (vii) $-x+1, -y, -z$; (viii) $-x+1, y, -z+\frac{1}{2}$; (ix) $-x+\frac{3}{2}, -y+\frac{1}{2}, -z$; (x) $-x+1, -y, -z+1$; (xi) $-x+1, -y+1, -z+1$; (xii) $-x+1, -y+1, -z+2$; (xiii) $-x+1, -y, -z+2$. † A prime is used to indicate the dimer's similarity to **D3** (see text).

a]pyridine and **odba** aromatic ring fragment and by $\pi\cdots\pi$ interactions between two imidazo[1,2-*a*]pyridine molecules. The total interaction energy characterizing the **X1** motif is about −70 kJ mol^{-1}. The other motif, **X2**, is held predominantly by weaker C—H$\cdots\pi$ contacts from the methoxy group to the **odba** aromatic ring fragment, and as such is less pronounced in terms of energy (*ca* −44 kJ mol^{-1}). The methoxy group is additionally engaged in a centrosymmetric motif linked via two C10—H10$\cdots$O1 interactions, although the interaction energy does not exceed −11 kJ mol^{-1} in this case.

Finally, the last crystal structure, *i.e.* **odba-d**, contains only two common motifs, **D1** and **D3**. The **D1** synthon is again comparable in energy with that observed in two above-described structures (*ca* −80 kJ mol^{-1}). In contrast, **D3**, which visually resembles the dimer found in the **odba-a** structure, is almost twice as energetically favoured as in the previous case, with an energy of about −72 kJ mol^{-1}.

Three other important motifs are present exclusively in this crystal structure, **X3**–**X5**. The **X3** dimer is centrosymmetric and bound by weak C—H$\cdots$O interactions between the acid and (*N*,*O*)-donor molecular fragments of the complex. The

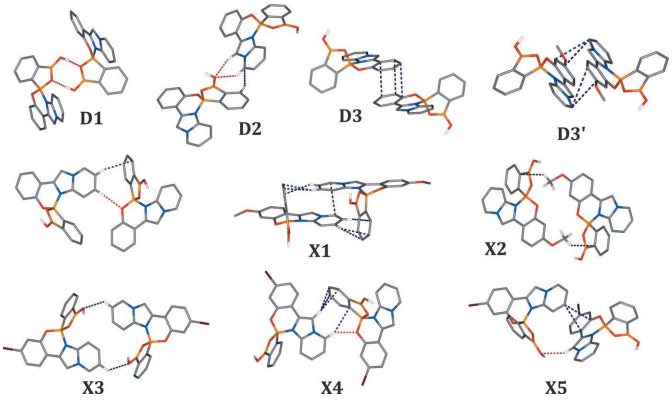

Figure 6
Selected motifs present in the crystal structures of the studied complexes. Note the **D**-type dimers are drawn based on the **odba-a** structure; **X1** and **X2** are present only in the **odba-b** structure, and **X3**, **X4** and **X5** are present only in the **odba-d** structure.

other two are asymmetric and formed via both C—H···O and C—H···π contacts. All three of these **X**-type motifs are described by similar interaction energies of about −54 kJ mol^{-1}. Interestingly, the bromine atoms are not very much involved in any specific contacts. Only some less specific long and weak C—H···Br, and perhaps Br···π [Br1···C5 = 3.695 (3) Å], contacts are encountered here, though clearly they do not dominate the crystal-structure formation and stability.

As far as cohesive energy is concerned, a comparison of the stability of the three crystal structures is not straightforward due to their various ASU contents. Therefore, to facilitate the analysis somewhat, the cohesive energy values gathered in Table 2 were calculated as averages per mole of single molecule, or of both molecule and the corresponding number of solvent species in the case of solvates. Additionally, the cohesive energies of the **odba-x** frameworks, that is excluding solvent, were evaluated. The cohesive energy obtained for the **odba-a** crystal structure is more advantageous than those evaluated for the other two structures, due to the most pronounced solvent contribution in that case. Regarding the energy of the crystal structure and its non-solvent equivalent, **odba-a** is most similar to the previously studied **odba** complexes with 8-hydroxyquinoline. In turn, **odba-b** is characterized by a more advantageous energy of the complex framework and a significantly lower solvent contribution. This results from the disordered acetone species (which interact non-optimally via the oxygen atom with both adjacent complex molecules), which lowers the solvent cohesive energy portion, and from the presence of a methoxy substituent containing an electronegative oxygen atom eager to form O···H interactions. In turn, the complex molecules themselves can be most favourably arranged in the case of **odba-d**, thus no solvent is needed to saturate the interactions.

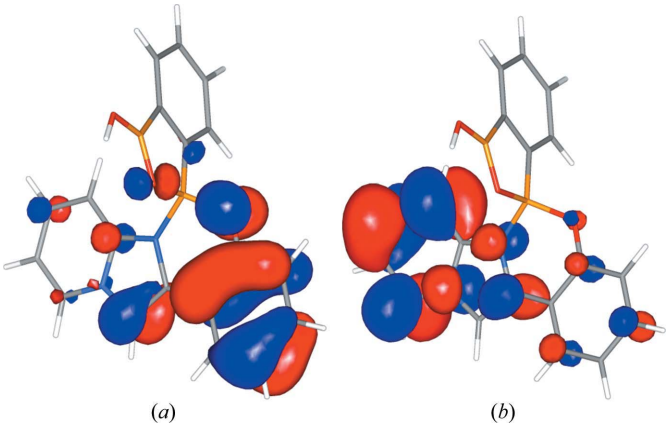

Figure 7
(*a*) HOMO and (*b*) LUMO orbitals for the **odba-a** molecule, calculated at the DFT(B3LYP)/6-311++G** level of theory (geometry optimized at the same level; isosurfaces drawn at 0.035 a.u, blue denotes positive and red negative).

3.4. Spectroscopic properties

Finally, the spectroscopic behaviour of the studied complexes was examined in solution and modelled theoretically to check the influence of complex formation on the absorption and emission properties of the respective imidazo[1,2-*a*]pyridines and the effect of the *R* and *R*′ substituents, if any.

The TDDFT results show that, for all complexes, the lowest energy singlet–singlet transition always involves the HOMO (highest occupied molecular orbital) and LUMO (lowest unoccupied molecular orbital) (Table 3S). These two molecular orbitals are centred almost exclusively on the imidazo[1,2-*a*]pyridine (Fig. 7, and Figs. 9S, 10S and 11S) and share nearly identical features in all the studied cases. The former observation is in contrast with that made for the previously published complexes of **odba** with 8-hydroxyquinoline (Jarzembska, Kamiński, Durka, Kubsik *et al.*, 2017),

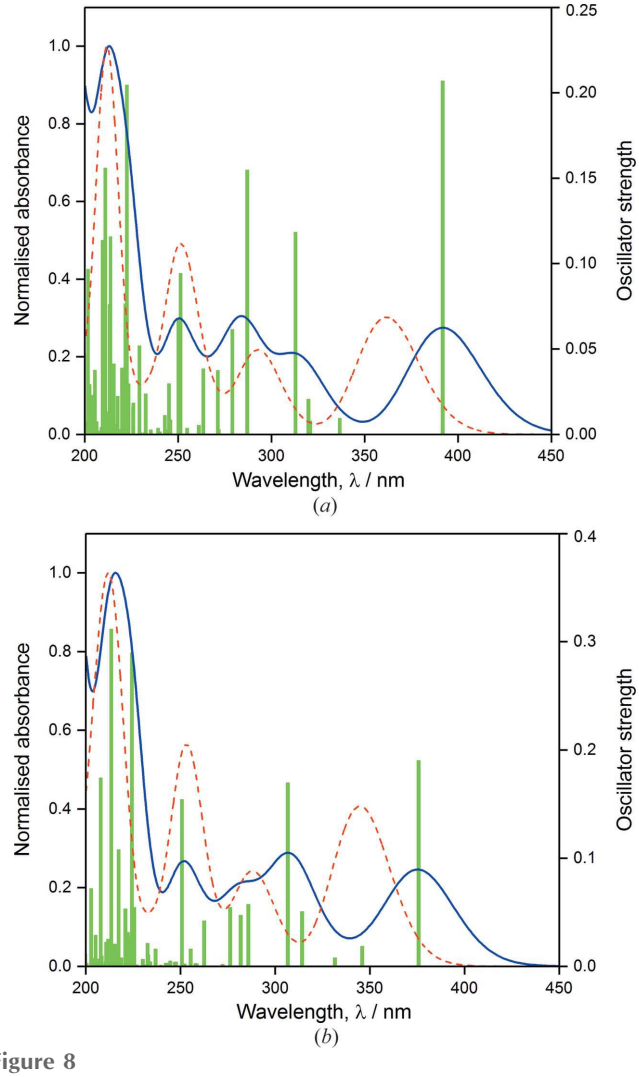

Figure 8
TDDFT-evaluated UV–Vis spectra [DFT(B3LYP)/6-311++G** level of theory] for (*a*) **odba-b** and (*b*) **odba-d** (optimized geometries). Oscillator strengths are marked as green bars. The blue-line envelope was drawn using the default *GAUSSSUM* program settings (the red-dashed-line envelopes are drawn for the free ligands **b** and **d**; for more information see the supporting information).

in which the HOMO-to-LUMO transition indicated charge transfer from the **odba** to the 8-oxyquinolinate fragment. In the case of the **odba-x** complexes considered here, only higher-energy transitions engaging HOMO-1, HOMO-2 and LUMO exhibit a charge-transfer nature, although they are significantly weaker than the HOMO-to-LUMO transition (Table 3S). It is also worth mentioning that, regarding the origin of the lowest-energy transitions, they are very much alike for all compounds despite their different phenyl-ring substituents. The most marked here is the **odba-b** complex with the methoxy substituent.

Concerning the absorption UV–Vis spectra, the TDDFT outcomes suggest a red shift of the absorption edge upon complexation (Fig. 8). According to this simulation, the effect is comparable for all studied compounds. Indeed, the collected solution absorption spectra confirm the similar behaviour of all compounds (Fig. 6S), for both the ligands and their complexes. A significant absorption band is in general observed within the near-UV region, whereas the complexation shifts the absorption edge slightly towards longer wavelengths. The effect is, however, much weaker than that indicated by the TDDFT results.

As far as the emission spectra are concerned (Fig. 9), the previously synthesized imidazo[1,2-*a*]pyridines, when excited, can undergo either typical relaxation to the ground state (*e.g.* fluorescence from a local excited state) or the already-mentioned ESIPT process, yielding different emission origins and thus different emission bands. The latter is associated with proton transfer across the intramolecular hydrogen bond and leads to a significant Stokes shift. In general, the way in which a molecule relaxes to the ground state depends on its environment. As previously studied by Stasyuk and co-workers (Stasyuk *et al.*, 2012; Stasyuk, Bultinck *et al.*, 2016), the ESIPT mechanism in imidazo[1,2-*a*]pyridines is well observed in aprotic solvents (*e.g.* toluene) and it can take place in polar aprotic solvents (*e.g.* acetonitrile), whereas proton transfer is blocked in polar protic solvents (*e.g.* methanol). In the case of the studied compounds, **a**, **b**, **c** and **d**, we confirmed these findings by collecting luminescence spectra for both toluene (non-polar aprotic) and acetone (polar aprotic) solutions. In the case of the **odba** complexes ESIPT is obviously not possible, thus only the regular relaxation can take place.

The spectra collected in toluene show that, when equimolar amounts of **odba** and the respective ligand are mixed, the

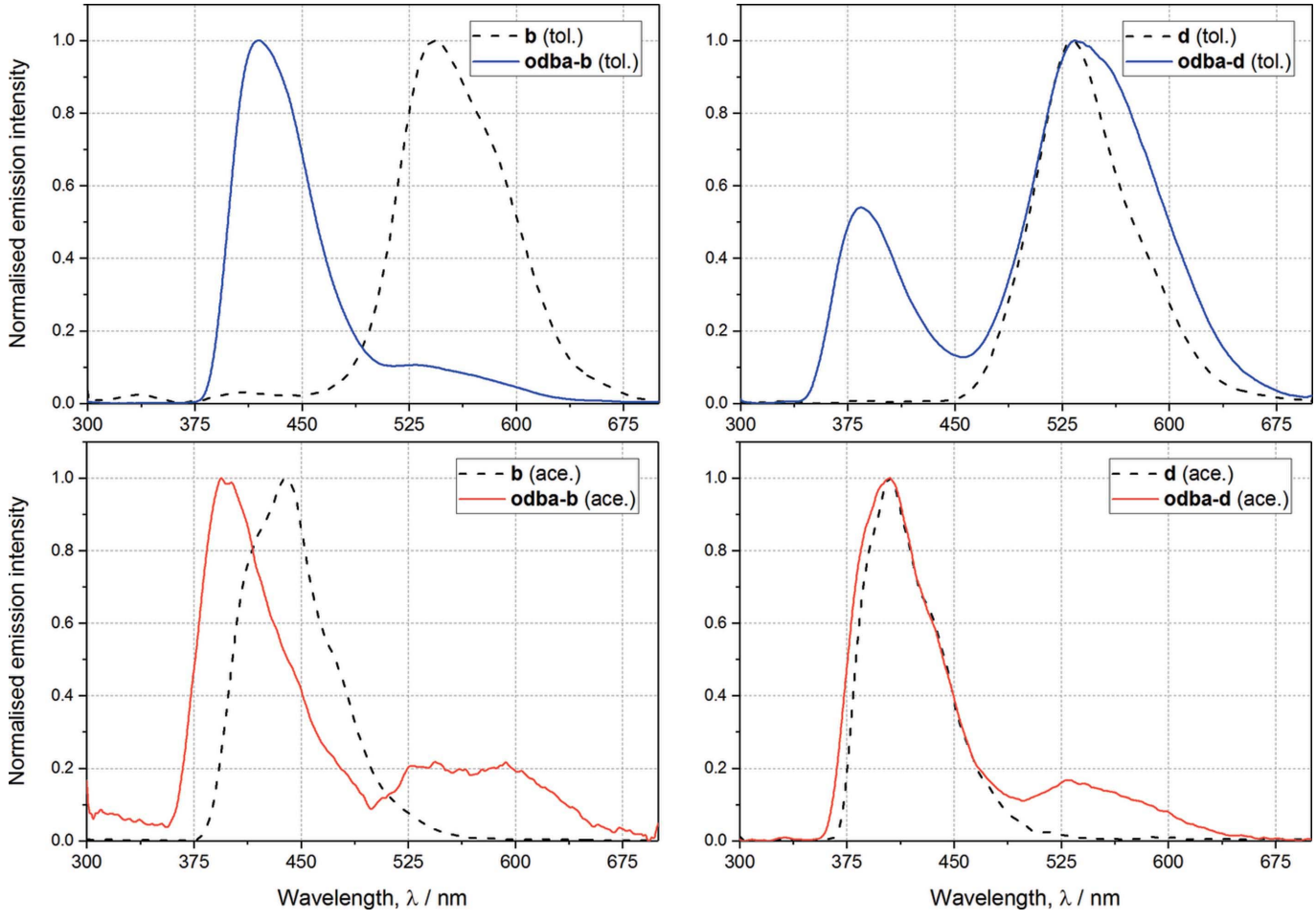

Figure 9
Experimental emission spectra for compounds **b** (left-hand panels) and **d** (right-hand panels) and their **odba** complexes measured in both toluene (top panels) (excitation wavelength λ_{ex} = 330 nm) and acetone (bottom panels) (λ_{ex} = 315 and 330 nm for **b** and **odba-b**, and **d** and **odba-d**, respectively).

reaction does not proceed completely (Fig. 9). Consequently, two emission bands can be distinguished: the ESIPT low-energy signal from the (*N*,*O*)-donor compound, and a high-energy peak attributed to the formed complex. Nevertheless, the ratios of both bands are different for each case. The conversion towards the desired complex is highest for **b** (the ESIPT band diminishes significantly) and it is visibly worse for **a**, whereas the bromine derivatives **c** and **d** convert to the least degree. Such behaviour can be assigned to the limited solubility of the examined compounds in toluene and to the equilibria reached under these conditions due to the different complexation constants depending on the *R* and *R*′ substituents.

A very different picture emerges for the acetone solutions (Fig. 9). In this case the reaction mixture exhibits a strong emission band around 390 nm coming from the complex, but there is also a wide and low-intensity band *ca* 525–600 nm. The near-UV signal is usually blue-shifted with respect to that of the imidazo[1,2-*a*]pyridine used, but much less significantly for the bromine derivatives. In turn, the weak low-energy band suggests that the ESIPT relaxation mechanism occurs for the free unreacted ligands (it is most pronounced in the cases of the **odba-b** and **odba-d** mixtures). Concerning the emission spectra of the free ligands, in the case of **a**, **b** and **d** the ESIPT band is not visible, while for compound **c** it clearly is (Fig. 8). This confirms that, in the case of acetone, both emission mechanisms can take place (unlike in methanol due to the formation of strong hydrogen bonds, but also much less readily than in aprotic polar acetonitrile). Thus, the complexation with **odba** most likely shifts the equilibrium in solution, or induces aggregation of free ligand molecules, facilitating the ESIPT process slightly.

Regarding the complex emission maxima, in general, two trends can be observed dependent on the solvent used. The emission maximum of the complexes in acetone varies around 400 nm and shifts towards longer wavelengths by about 15 nm in total, in the following order: **odba-a** < **odba-b** $\simeq$ **odba-c** < **odba-d**. A different trend is observed for the toluene solutions, in which the maximum varies around 410 nm and **odba-a** and **odba-b** exhibit quite similar maximum positions (about 413 nm), while the maximum of **odba-d** is the most blue-shifted in the series. In this case the peak maximum wavelength sequence is as follows: **odba-d** < **odba-a** $\simeq$ **odba-c** < **odba-b**, with an overall interval of about 25 nm. These trends differ from those observed for the parent compounds **a**, **b**, **c** and **d**. Thus, some effect of the substituent is visible, although it varies depending on the solvent and the level of complexation.

4. Summary and conclusions

In this contribution four new blue-luminescent *ortho*-phenylenediboronic acid complexes with a series of 2-(2′-hydroxyphenyl)imidazo[1,2-*a*]pyridine derivatives are reported. Three of them were crystallized successfully and their crystal structures have been determined, *i.e.* the complex containing the parent (*N*,*O*)-donor ligand **a** (*R* = *R*′ = H), and its methoxy- and bromine-substituted analogues, **odba-b** (*R* = H, *R*′ = OMe) and **odba-d** (*R* = Br, *R*′ = H), respectively. These compounds form different crystal architectures in terms of the ASU content and packing. Nevertheless, the **odba-a** and **odba-b** solvates resemble to some extent the previously published structures of **odba** with 8-hydroxyquinoline (Jarzembska, Kamiński, Durka, Kubsik *et al.*, 2017). Additionally, all the crystal structures contain a typical centrosymmetric **D1** motif, formed by interactions between the boronic groups, and are stabilized by various advantageous π-stacking interactions. In the case of **odba-a**, the solvent plays an important role in the energetic stability of the crystal structure. However, the acetone molecules are disordered in the **odba-b** crystal, resulting in a less pronounced solvent contribution to the cohesive energy in that case. On the other hand, the **odba-b** solvent-free framework, supported by methoxy group interactions, is much better stabilized than that created by **odba-a**. Also, in the case of the imidazo[1,2-*a*]pyridine derivative crystals, the methoxy group makes a difference. However, it does not lead here to a more advantageous cohesive energy of the crystal (**b**), but to a significantly different crystal packing from the fluorine, bromine (**c**) and methyl derivatives (these two last compounds form isostructural crystal structures). It should also be noted that the examined (*N*,*O*)-donor compounds do not form any very specific or strong interactions, which is reflected in their moderate cohesive energy values. This supports the preferred crystallization of the complex species from solution with respect to the (*N*,*O*)-donor compounds used, as the former systems create more energetically advantageous crystal networks (taking into consideration also the energies of the complex frameworks). Of course, in some cases kinetic and entropic factors are crucial for crystallization to occur.

Finally, the spectroscopic properties of the new complexes were examined. TDDFT computations showed that, in contrast with the 8-oxyquinolinate analogues, the lowest energy transitions in **odba-x** occur predominantly on the (*N*,*O*)-donor fragment and thus do not lead to a charge-transfer process. Consequently, the spectroscopic behaviour of the series is very much comparable with that of the 2-arylimidazo[1,2-*a*]pyridines incapable of ESIPT, as shown by the absorption and emission spectra collected in toluene and acetone solutions. Complexation causes a reduction in the Stokes shift compared with that of the respective (*N*,*O*)-donor molecules. The emission spectroscopy of the free ligands confirms what has been previously reported by Stasyuk *et al.* (2012). Indeed, in an aprotic non-polar solvent (toluene) the ESIPT band is very pronounced. However, in an aprotic but polar solvent (acetone) the ESIPT band does not appear. Interestingly, the addition of **odba** to a solution of the ligand in acetone enhances the ESIPT band (which is in general not visible for the ligand solution itself), which may be attributed to the shifted equilibria or to possible aggregation of free ligand molecules.

The phenyl-ring substituents clearly influence the crystallization process, the molecular packing in the solid state and the spectroscopic properties of the examined compounds,

mainly via governing the nature of the complex–solvent interactions. Nevertheless, more investigations should be undertaken to draw binding conclusions in this matter.

Acknowledgements

Sylwia Kutniewska, Katarzyna Jarzembska and Radosław Kamiński would like to thank Krzysztof Durka (Warsaw, Poland) for providing the *ortho*-phenylenediboronic acid. The authors declare no competing financial interests.

Funding information

Sylwia Kutniewska and Katarzyna Jarzembska are grateful for financial support through a SONATA grant (No. 2014/15/D/ST4/02856) from the National Science Centre in Poland. The authors thank the Wrocław Centre for Networking and Supercomputing (grant No. 285) and the Interdisciplinary Centre for Mathematical and Computational Modelling (grant No. G33-14) for providing computational facilities.

References

Abignente, E. (1991). *Actual. Chim. Ther.* **18**, 193–214.
Adamo, C. & Barone, V. (1999). *J. Chem. Phys.* **110**, 6158–6170.
Alibabaei, L., Luo, H., House, R. L., Hoertz, P. G., Lopez, R. & Meyer, T. J. (2013). *J. Mater. Chem. A*, **1**, 4133–4145.
Allen, F. H. & Bruno, I. J. (2010). *Acta Cryst.* B**66**, 380–386.
Allen, F. H., Kennard, O., Watson, D. G., Brammer, L., Orpen, A. G. & Taylor, R. (1987). *J. Chem. Soc. Perkin Trans. 2*, pp. S1–S19.
An, W., Wang, W., Yu, T., Zhang, Y., Miao, Z., Meng, T. & Shen, J. (2016). *Eur. J. Med. Chem.* **112**, 367–372.
Anderson, S., Weaver, M. S. & Hudson, A. J. (2000). *Synth. Met.* **111–112**, 459–463.
Authier, A. (2014). Editor. *International Tables for Crystallography*, Vol. D, *Physical Properties of Crystals*, 2nd ed. Chester: International Union of Crystallography.
Balijapalli, U. & Iyer, S. K. (2015). *Dyes Pigm.* **121**, 88–98.
Becke, A. D. (1988). *Phys. Rev. A*, **38**, 3098–3100.
Boys, S. F. & Bernardi, F. (1970). *Mol. Phys.* **19**, 553–566.
Bruker (2015). *APEX3*. Bruker AXS, Madison, Wisconsin, USA.
Clark, T., Chandrasekhar, J., Spitznagel, G. W. & Schleyer, P. (1983). *J. Comput. Chem.* **4**, 294–301.
Corona, L. D., Pellegatta, C., Signorelli, G., Buran, V., Massaroli, G., Turba, C., Faini, D. & Pagella, P. G. (1981). *Farmaco Sci.* **36**, 994–1003.
Cui, Y. & Wang, S. (2006). *J. Org. Chem.* **71**, 6485–6496.
Desiraju, G. R. & Sarma, J. A. R. P. (1986). *Proc. Indian Acad. Sci. Chem. Sci.* **96**, 599–605.
Dill, J. D. & Pople, J. A. (1975). *J. Chem. Phys.* **62**, 2921–2923.
Dominiak, P. M., Volkov, A., Li, X., Messerschmidt, M. & Coppens, P. (2007). *J. Chem. Theor. Comput.* **3**, 232–247.
Dovesi, R., Orlando, R., Civalleri, B., Roetti, C., Saunders, V. R. & Zicovich-Wilson, C. M. (2005). *Z. Kristallogr.* **220**, 571–573.
Dovesi, R., Saunders, V. R., Roetti, C., Orlando, R., Zicovich-Wilson, C. M., Pascale, F., Civalleri, B., Doll, K., Harrison, N. M., Bush, I. J., D'Arco, P. & Llunell, M. (2009). *CRYSTAL09*. University of Turin, Italy.
Durka, K., Jarzembska, K. N., Kamiński, R., Luliński, S., Serwatowski, J. & Woźniak, K. (2013). *Cryst. Growth Des.* **13**, 4181–4185.
Durka, K., Lulinski, S., Jarzembska, K. N., Smetek, J., Serwatowski, J. & Wozniak, K. (2014). *Acta Cryst.* B**70**, 157–171.
Edwards, M. R., Jones, W., Motherwell, W. D. S. & Shields, G. P. (2001). *Mol. Cryst. Liq. Cryst. Sci. Technol.* **356**, 337–353.
Etter, M. C. (1990). *Acc. Chem. Res.* **23**, 120–126.
Frisch, M. J., Trucks, G. W., Schlegel, H. B., Scuseria, G. E., Robb, M. A., Cheeseman, J. R., Scalmani, G., Barone, V., Mennucci, B., Petersson, G. A., Nakatsuji, H., Caricato, M., Li, X., Hratchian, H. P., Izmaylov, A. F., Bloino, J., Zheng, G., Sonnenberg, J. L., Hada, M., Ehara, M., Toyota, K., Fukuda, R., Hasegaw, J., Ishida, M., Nakajima, T., Honda, Y., Kitao, O., Nakai, H., Vreven, T. J. A., Montgomery, J., Peralta, J. E., Ogliaro, F., Bearpark, M., Heyd, J. J., Brothers, E., Kudin, K. N., Staroverov, V. N., Kobayashi, R., Normand, J., Raghavachari, K., Rendell, A., Burant, J. C., Iyengar, S. S., Tomasi, J., Cossi, M., Rega, N., Millam, J. M., Klene, M., Knox, J. E., Cross, J. B., Bakken, V., Adamo, C., Jaramillo, J., Gomperts, R., Stratmann, R. E., Yazyev, O., Austin, A. J., Cammi, R., Pomelli, C., Ochterski, J. W., Martin, R. L., Morokuma, K., Zakrzewski, V. G., Voth, G. A., Salvador, P., Dannenberg, J. J., Dapprich, S., Daniels, A. D., Farkas, Ö., Foresman, J. B., Ortiz, J. V., Cioslowski, J. & Fox, D. J. (2009). *GAUSSIAN09*. Gaussian Inc., Wallingford, CT, USA.
Grätzel, M. (2009). *Acc. Chem. Res.* **42**, 1788–1798.
Grimme, S. (2004). *J. Comput. Chem.* **25**, 1463–1473.
Grimme, S. (2006). *J. Comput. Chem.* **27**, 1787–1799.
Grimme, S., Antony, J., Ehrlich, S. & Krieg, H. (2010). *J. Chem. Phys.* **132**, 154104.
Grimme, S., Ehrlich, S. & Goerigk, L. (2011). *J. Comput. Chem.* **32**, 1456–1465.
Groom, C. R., Bruno, I. J., Lightfoot, M. P. & Ward, S. C. (2016). *Acta Cryst.* B**72**, 171–179.
Gueiffier, A., Mavel, S., Lhassani, M., Elhakmaoui, A., Snoeck, R., Andrei, G., Chavignon, O., Teulade, J.-C., Witvrouw, M., Balzarini, J., De Clercq, E. & Chapat, J.-P. (1998). *J. Med. Chem.* **41**, 5108–5112.
Hansen, N. K. & Coppens, P. (1978). *Acta Cryst.* A**34**, 909–921.
Hariharan, P. C. & Pople, J. A. (1973). *Theor. Chim. Acta*, **28**, 213–222.
Hehre, W. J., Ditchfield, R. & Pople, J. A. (1972). *J. Chem. Phys.* **56**, 2257–2261.
Jarzembska, K. N. & Dominiak, P. M. (2012). *Acta Cryst.* A**68**, 139–147.
Jarzembska, K. N., Hoser, A. A., Kamiński, R., Madsen, A. Ø., Durka, K. & Woźniak, K. (2014). *Cryst. Growth Des.* **14**, 3453–3465.
Jarzembska, K. N., Kamiński, R., Durka, K. & Kubsik, M. (2017). *Cryst. Growth Des.* **17**, 6836–6851.
Jarzembska, K. N., Kamiński, R., Durka, K., Kubsik, M. & Nawara, K. (2015). *Acta Cryst.* A**71**, s333.
Jarzembska, K. N., Kamiński, R., Durka, K., Kubsik, M., Nawara, K., Witkowska, E., Wiloch, M., Luliński, S., Waluk, J., Głowacki, I. & Woźniak, K. (2017). *Dyes Pigm.* **138**, 267–277.
Jarzembska, K. N., Kubsik, M., Kamiński, R., Woźniak, K. & Dominiak, P. M. (2012). *Cryst. Growth Des.* **12**, 2508–2524.
Kaminski, R., Jarzembska, K. N. & Domagala, S. (2013). *J. Appl. Cryst.* **46**, 540–543.
Kamtekar, K. T., Monkman, A. P. & Bryce, M. R. (2010). *Adv. Mater.* **22**, 572–582.
Kappaun, S., Rentenberger, S., Pogantsch, A., Zojer, E., Mereiter, K., Trimmel, G., Saf, R., Möller, K. C., Stelzer, F. & Slugovc, C. (2006). *Chem. Mater.* **18**, 3539–3547.
Knox, J. E., Halls, M. D., Hratchian, H. P. & Schlegel, H. B. (2006). *Phys. Chem. Chem. Phys.* **8**, 1371–1377.
Krishnan, R., Binkley, J. S., Seeger, R. & Pople, J. A. (1980). *J. Chem. Phys.* **72**, 650–654.
Lee, C., Yang, W. & Parr, R. G. (1988). *Phys. Rev. B*, **37**, 785–789.
Li, H. & Jäkle, F. (2009). *Macromolecules*, **42**, 3448–3453.
Lin, N., Qiao, J., Duan, L., Xue, J. & Wang, L. (2014). *Chem. Mater.* **26**, 3693–3700.
Luliński, S., Smętek, J., Durka, K. & Serwatowski, J. (2013). *Eur. J. Org. Chem.* pp. 8315–8322.
Macchi, P. & Coppens, P. (2001). *Acta Cryst.* A**57**, 656–662.
Márquez-Flores, Y. K., Campos-Aldrete, E., Salgado-Zamora, H., Correa-Basurto, J. & Meléndez-Camargo, E. (2012). *Med. Chem. Res.* **21**, 3491–3498.

McLean, A. D. & Chandler, G. S. (1980). *J. Chem. Phys.* **72**, 5639–5648.
Mondal, S., Prathapa, S. J. & van Smaalen, S. (2012). *Acta Cryst.* A**68**, 568–581.
Mutai, T., Ohkawa, T., Shono, H. & Araki, K. (2016). *J. Mater. Chem. C*, **4**, 3599–3606.
Mutai, T., Sawatani, H., Shida, T., Shono, H. & Araki, K. (2013). *J. Org. Chem.* **78**, 2482–2489.
Mutai, T., Shono, H., Shigemitsu, Y. & Araki, K. (2014). *CrystEngComm*, **16**, 3890–3895.
Mutai, T., Tomoda, H., Ohkawa, T., Yabe, Y. & Araki, K. (2008). *Angew. Chem. Int. Ed.* **47**, 9522–9524.
Nagata, Y. & Chujo, Y. (2008). *Macromolecules*, **41**, 2809–2813.
O'Boyle, N. M., Tenderholt, A. L. & Langner, K. M. (2008). *J. Comput. Chem.* **29**, 839–845.
Oszlányi, G. & Sütő, A. (2004). *Acta Cryst.* A**60**, 134–141.
Oszlányi, G. & Sütő, A. (2005). *Acta Cryst.* A**61**, 147–152.
Palatinus, L. (2013). *Acta Cryst.* B**69**, 1–16.
Palatinus, L. & Chapuis, G. (2007). *J. Appl. Cryst.* **40**, 786–790.
Peintinger, M. F., Oliveira, D. V. & Bredow, T. (2013). *J. Comput. Chem.* **34**, 451–459.
Perdew, J. P. (1986). *Phys. Rev. B*, **33**, 8822–8824.
Perdew, J. P., Burke, K. & Ernzerhof, M. (1996). *Phys. Rev. Lett.* **77**, 3865–3868.
Petříček, V., Dušek, M. & Palatinus, L. (2014). *Z. Kristallogr.* **229**, 345–352.
Qin, Y., Kiburu, I., Shah, S. & Jäkle, F. (2006). *Org. Lett.* **8**, 5227–5230.
Ribeiro, I. G., da Silva, K. C. M., Parrini, S. C., de Miranda, A. L. P., Fraga, C. A. M. & Barreiro, E. J. (1998). *Eur. J. Med. Chem.* **33**, 225–235.
Salunke, D. B., Yoo, E., Shukla, N. M., Balakrishna, R., Malladi, S. S., Serafin, K. J., Day, V. W., Wang, X. & David, X. (2012). *J. Med. Chem.* **55**, 8137–8151.
Simon, S., Duran, M. & Dannenberg, J. J. (1996). *J. Chem. Phys.* **105**, 11024–11031.
Spackman, M. A. (2013). *Phys. Scr.* **87**, 048103.
Spackman, M. A. & Jayatilaka, D. (2009). *CrystEngComm*, **11**, 19–32.
Starr, J. T., Sciotti, R. J., Hanna, D. L., Huband, M. D., Mullins, L. M., Cai, H., Gage, J. W., Lockard, M., Rauckhorst, M. R., Owen, R. M., Lall, M. S., Tomilo, M., Chen, H., McCurdy, S. P. & Barbachyn, M. R. (2009). *Bioorg. Med. Chem. Lett.* **19**, 5302–5306.
Stasyuk, A. J., Banasiewicz, M., Cyrański, M. K. & Gryko, D. T. (2012). *J. Org. Chem.* **77**, 5552–5558.
Stasyuk, A. J., Bultinck, P., Gryko, D. T. & Cyrański, M. K. (2016). *J. Photochem. Photobiol. Chem.* **314**, 198–213.
Stasyuk, A. J., Cywiński, P. J. & Gryko, D. T. (2016). *J. Photochem. Photobiol. Photochem. Rev.* **28**, 116–137.
Su, Z. & Coppens, P. (1998). *Acta Cryst.* A**54**, 646–652.
Volkov, A., Li, X., Koritsanszky, T. & Coppens, P. (2004). *J. Phys. Chem. A*, **108**, 4283–4300.
Wang, X.-Y. & Weck, M. (2005). *Macromolecules*, **38**, 7219–7224.
Wesela-Bauman, G., Ciećwierz, P., Durka, K., Luliński, S., Serwatowski, J. & Woźniak, K. (2013). *Inorg. Chem.* **52**, 10846–10859.
Wu, Y., Yuan, W., Ji, H., Qin, Y., Zhang, J., Li, H., Li, Y., Wang, Y., Sun, Y. & Liu, W. (2017). *Dyes Pigm.* **142**, 330–339.
Zhao, Y. H., Abraham, M. H. & Zissimos, A. M. (2003). *J. Org. Chem.* **68**, 7368–7373.